Petruzzelli F., Della Corte G., Iervolino I. (2012) Seismic Risk Assessment of an Industrial Steel Building Part 2: Fragility and Failure Probabilities. Proc of. 15WCEE, Lisboa, PT. Paper No. 3088.

Seismic Risk Assessment of an Industrial Steel Building Part 2: Fragility and Failure Probabilities

F. Petruzzelli, I. Iervolino & G. Della Corte
Università degli Studi di Napoli Federico II, Italy

SUMMARY:
This paper describes the probabilistic framework used to assess the seismic risk of an existing industrial steel building, in the framework of performance-based earthquake engineering. The risk assessment is based on incremental dynamic inelastic analyses, carried out on structural models described in a companion paper. Seismic hazard at the site of interest and the associated selection of ground motion acceleration records, on the basis of design earthquakes from disaggregation, are addressed first. Subsequently, fragility curves, related to the structural behaviour only, are obtained for different limit states of industrial interest. The results of the application of this framework are represented by the probabilities of failure for different limit states, which represents a basis for further evaluation regarding expected loss assessment.

Keywords: Collapse, Disaggregation, Existing structures, Expected loss, Hazard.

1. INTRODUCTION

This paper presents applications, to an existing industrial steel building, of performance-based earthquake engineering methods. Although it is known that damage to contents and non-structural components represents most of the losses in seismic events, in this paper the occurrence of structural failure is addressed, as it is the basis for any loss assessment, which would include seismic behaviour of non-structural elements and content. In fact, outcome of the work is the assessment of probabilities of failure corresponding to different structural performances.
A schematic plan view of the building is shown in Figure 1, with the analysed three-dimensional and bi-dimensional finite element models. Considering the different portions of the building, one three-dimensional model ("1991-3D") and four bi-dimensional models ("1971/79-2D-X", "1971/79-2D-Y", "1991-2D-X" and "1991-2D-Y") were analysed. The risk assessment is based on incremental dynamic inelastic analyses (IDAs, Vamvatsikos and Cornell, 2002), whose results are expressed both in terms of peak transient drift (global engineering demand parameters) and force demand to individual members and connections (local engineering demand parameters). Force demand is monitored to control the occurrence of local undesired failure modes, such as failure of roof members or connections, and failure of column base plate welded connections. Such existing structures, in fact, are often characterised by non-standard detailing due to a design performed in the absence of any capacity design prescription. Therefore, the quantification of probabilities of failure due to both global sidesway collapse and local mechanisms is required.
Seismic hazard at the building site, whose location is not explicitly mentioned because of confidentiality agreement with the stakeholder, has been specifically assessed taking into account local site conditions. Acceleration records have been subsequently selected on the basis of a disaggregation analysis in terms of earthquake magnitude and site-to-source distance. The seismic vulnerability is expressed, for each limit state under consideration, by means of fragility curves. For each of the analysed structures, the integration of seismic hazard and vulnerability led to failure probabilities corresponding to different limit states, for both global and local failure modes. This information, properly integrated with a cost analysis, which is beyond the scope of this work, represents a basis for the evaluation of annual expected losses and for the identification of priorities of intervention for structural retrofitting.

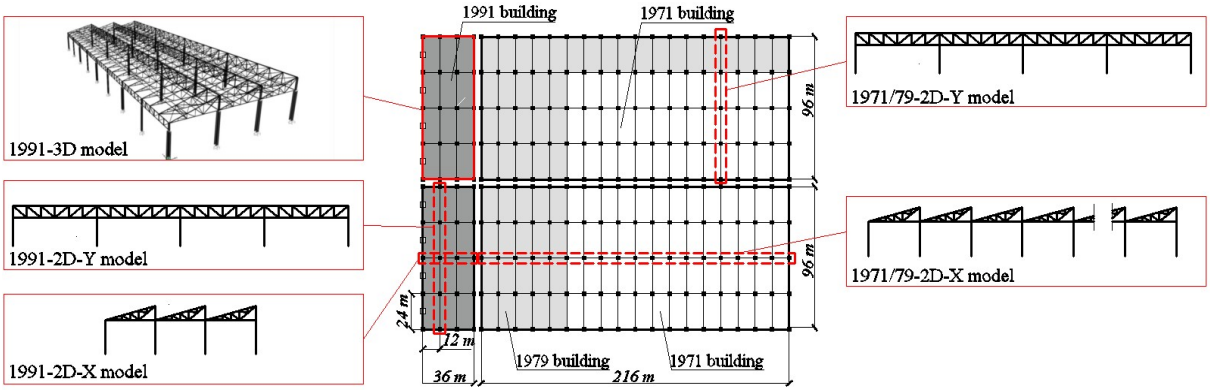

Figure 1. Plan view of case study building and analysed structural models

2. METHODOLOGY

Probabilistic performance objectives considered in this paper are the three limit states frequently adopted within the PBEE framework (Cornell and Krawinkler, 2000), namely, immediate occupancy (IO), life safety (LS) and collapse prevention (CP) (FEMA, 2000). These performance objectives are identified in this study by taking into account the uncertainty in ground motion, while structural capacity is assumed to be deterministic. For any given limit state, the probability of failure (P_f) is generally expressed as follows:

$$P_f = \int_x P[failure \mid x] \cdot f_{IM}(x)\, dx \tag{2.1}$$

where *IM* denotes the chosen ground motion intensity measure (peak ground or spectral acceleration in the most simple cases) and *P[failure|x]* is the probability that the demand exceeds the capacity (also known as fragility), for a given level of intensity measure $IM = x$. Generally, both the capacity and the demand are expressed in terms of a selected engineering demand parameter (*EDP*, e.g. maximum interstorey drift ratio, internal action in members and connections). $f_{IM}(x)$ is the probability density function of the chosen IM, obtained from a probabilistic seismic hazard analysis for the site of interest. An important advantage of this approach is that the evaluation of earthquake consequences is decomposed in subtasks for seismologists, structural engineers, loss analysts or stakeholders (evaluation of losses related to each limit state). The expected loss (*E[l]*) can finally be expressed as given by Equation (2.2), provided that one is able to associate the expected consequences to any given limit state.

$$E[l] = E[l \mid failure] \cdot P_f \tag{2.2}$$

In the following, the calculations and the main assumptions made for the definition of the terms of Equation (2.1) are discussed.

3. SEISMIC HAZARD

3.1. Hazard curves

According to the seismic classification of the Italian territory (CS.LL.PP., 2008), the building site is characterized by a peak ground acceleration (PGA) on rock, equal to 0.26 g corresponding to a return period of 475 years. According to the same code, the foundation soil is classified as type B, which is characterized by a shear wave velocity in the range of 360 m/s to 800 m/s within the first thirty meters

of depth from the ground surface. For the purposes of the implementation of IDAs, the spectral acceleration at the fundamental period of the structure, $S_a(T_1)$, has been adopted as the intensity measure (Shome *et al.*,1998).
Seismic hazard was evaluated specifically for the building site. Using the same source model implemented in the official Italian seismic hazard map, site-specific hazard curves were computed in terms of spectral accelerations at vibration periods of 1 s and 1.6 s, which are characteristics of the analyzed structures. The corresponding seismic hazard curves are plotted in Figure 2. A detailed description of the calculation method can be found in Iervolino *et al.* (2011).

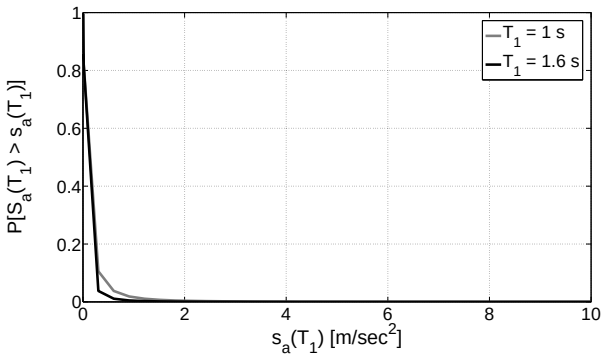

Figure 2. Exceedance probabilities for soft soil in 1 year at the site, for the IMs of interest.

3.2. Ground motion record selection

The selection of the ground motion acceleration records, to be used in time-history nonlinear analyses, was performed based on a disaggregation of the seismic hazard, described at Section 3.1. In particular, to ensure consistency between the selected accelerograms and the seismic hazard at different levels of intensity, four levels of the adopted IM were considered first, corresponding to a return period equal to 50, 475, 975 and 2475 years, respectively. For each level of intensity, disaggregation in terms of earthquake moment magnitude and site-to-source epicentral distance was performed, using the software tools described in Iervolino *et al.* (2011). As an example, Figures 3 and 4 show the results of the disaggregation analysis for the spectral acceleration at 1 s (Figs. 3*a* and 4*a*) and 1.6 s (Figs. 3*b* and 4*b*) and a return period equal to 475 and 2475 years, respectively. The disaggregation leads in both cases to a distribution with a single mode; i.e., one source zone dominates the hazard for the site.
Once values of magnitude and distance that mostly contribute to the seismic hazard at the site were determined, thirty real ground acceleration records were selected, for each of the considered levels of seismic intensity. The selection was made with the aid of REXEL (Iervolino *et al.*, 2010), searching for records in both the Italian (ITACA, ITalian ACcelerometric Archive) and European (ESD, European Strong-Motion Database) databases. Table 1 shows the criteria adopted for selecting the records. For any given return period and corresponding spectral acceleration, ranges of values of magnitude and distance are given. Looking at Table 1, it can be seen that different magnitudes and distances characterize earthquakes producing different levels of spectral accelerations (second column of Table 1) and associated to different return periods (first column of Table 1). Since acceleration records produced by real earthquakes are intended to be used, different sets need to be searched for different levels of spectral acceleration by looking at historical earthquakes satisfying the magnitude-distance requirements of Table 1.
In the range of spectral accelerations identified by two subsequent levels in Table 1, the acceleration records found for the lower bound level have been used, by scaling accelerations until the upper bound acceleration level of the range has been reached. It may be worth noting that the three-dimensional model (1991-3D model) was analysed for spectral accelerations ranging from 0.1 to 1 g, while 2D models were analysed for $S_a(T_1)$ between 0.1 and 3 g. The smaller range of $S_a(T_1)$ in case of a 3D model was due to the larger computational efforts in comparison with the 2D models. However, as it will be discussed in the following, this limitation in the range of values of $S_a(T_1)$ is considered to be not detrimental to the analysis of failure probabilities.

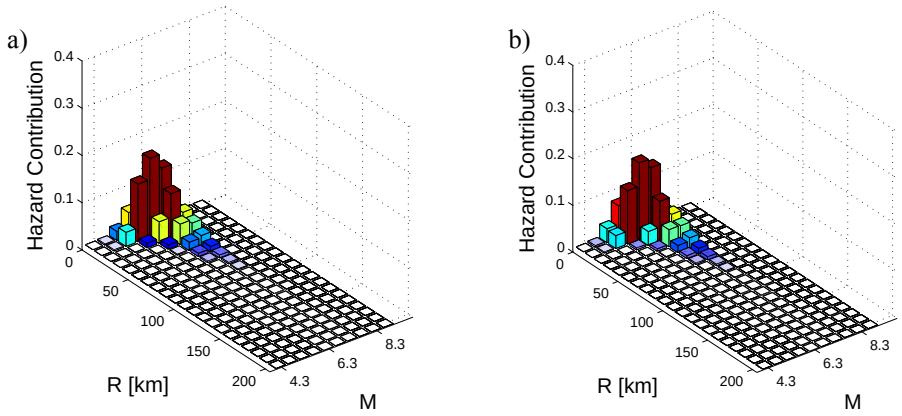

Figure 3. Seismic hazard disaggregation of $S_a(T_1)$, for T_1 = 1.0 s (a) and 1.6 s (b), for 475 yrs return period.

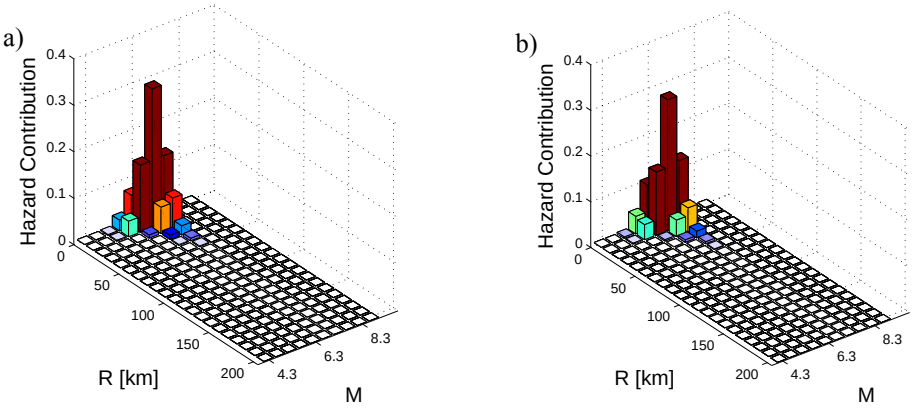

Figure 4. Seismic hazard disaggregation of $S_a(T_1)$, for T_1 = 1.0 s (a) and 1.6 s (b), for 2475 yrs return period.

Table 1. Results of seismic hazard disaggregation as used for record selection.

T_R [yrs]	$S_a(T_1)$ [g]	R [km]	M	Database
50	0.10	0 – 20	5 – 6	ITACA
475	0.30	0 – 30	5.3 – 6.5	ITACA
975	0.37	5 – 25	6 – 7	ESD
2475	0.50	0 – 40	6 – 7.5	ESD

4. SEISMIC DEMAND ANALYSIS

4.1 Global analysis (drift demand)

This Section presents a short summary of the nonlinear dynamic analyses, which were carried out in order to statistically characterize seismic demand to the case-study structures. More details can be found in the companion paper (Petruzzelli *et al.*, 2012). The structural behaviour was investigated by means of IDA. The assumed *EDPs* are the peak transient roof drift ratio, which is used as a measure of the global structural performance, and the peak transient member force demand, which is used to control the event of any local failure mode. As discussed in the companion paper, the roof drift capacity is taken as suggested by FEMA 356 regulations (ASCE, 2000) and corresponding to the three limit states of IO, LS and CP. Figure 5 illustrates the median drift ratio demand and the capacity limits corresponding to the three considered limit states (δ_{IO}, δ_{LS} and δ_{CP}). As discussed in Petruzzelli *et al.* (2012), a global sidesway collapse mechanism was considered to be developed when the drift demand resulted to be larger than a drift capacity, δ_U. In this study, δ_U was evaluated as the drift corresponding

to a zero lateral strength from a pushover analysis, but reduced of a factor 0.5 which is introduced to take approximately into account the effect of local strength degradation at plastic zones. Therefore, any acceleration record producing a drift demand larger than δ_U is considered to produce global collapse; the corresponding drift demand is removed from the statistics of data, but it is taken into account as a separate contribution to evaluate the failure probability. This aspect will be discussed at Section 5, while it is here sufficient to note that this removal of the collapse case is the reason why the median response curve shown in Figure 5 seems to be characterized by a vertical asymptote.

4.2 Local analyses (internal force demand)

In the examined structures, failure of roof members and connections, as well as weld failure at column base connections may occur. These failure modes should generally be avoided, because of either their brittle nature (weld failure) or the serious consequences (roof collapse under gravity loads). Therefore, force demand to these structural elements were compared with the corresponding force capacity, the latter obtained as the minimum over any possible local failure mode. Figure 5*b* shows one example of axial force demand to one roof member and relevant end connections belonging to the "1991-2D-Y" structure, together with the capacity, N_{CAP}. The median force demand curve, plotted in Figure 5*b* with a black bold line, tends to exhibit a vertical asymptote. This is due to the formation of a fully plastic collapse mechanism (plastic hinges at the top and bottom of each column end). A slight increase of force demand may still occur after the formation of this plastic mechanism because the roof mass was distributed to also the upper chord joints. Moreover, the roof truss members are modelled as linear elastic in the analysis.

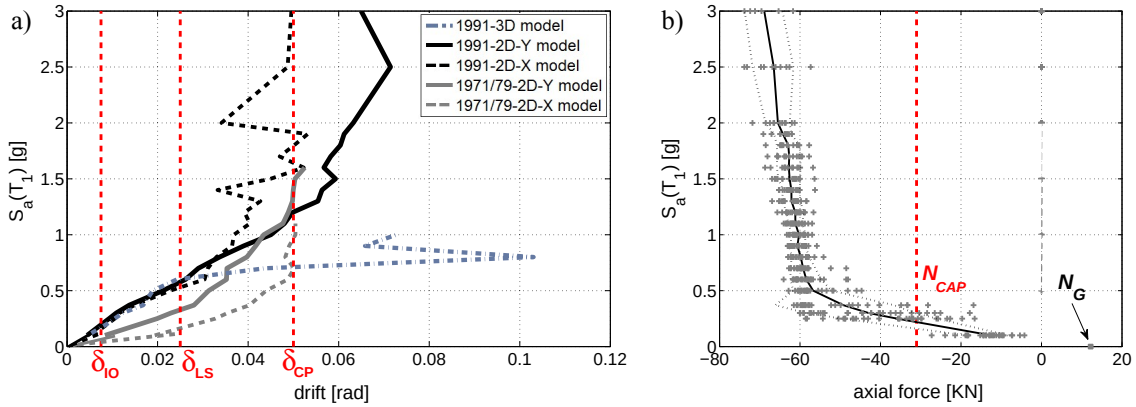

Figure 5. (a) Median of global drift ratios for "non-collapse" cases and capacity limits corresponding to different limit states; (b) local force demand in one member and corresponding axial force capacity, N_{CAP}.

5. FRAGILITY CURVES

5.1 Global failure modes (drift fragility)

At a given level of spectral acceleration, the distribution of drift demand over the considered acceleration records allows one to calculate the probability of exceeding a given drift capacity. The probability that the demand exceeds the capacity, in the whole field of the intensity measure, is the fragility. This probability can be estimated either from the number of failures out of the total number of cases, or fitting a probability distribution of demands for each level of the intensity measure.
The probabilities of exceeding the IO and LS limit states were computed by fitting a log-normal distribution to the global drift demands at each IM level. The fitting was based on estimated values of median and standard deviation, obtained from the IDA results (Fig. 5a).
As discussed at Section 4.1, drift demands larger than the limit value δ_U are considered as cases of global collapse. Such values are not included in the calculation of statistics for the lognormal distribution, because it is assumed that the structure is unstable if the limit δ_U is exceeded.

The events $\delta > \delta_U$ are included as separate contributions for calculating failure probabilities, by means of Equation (5.1), according to Shome and Cornell (2000).

$$P[\,failure \mid x] = P[\,failure \mid x, NC] \cdot P\big[NC \mid x\big] + P[\,failure \mid x, C] \cdot \big(1 - P\big[NC \mid x\big]\big) \tag{5.1}$$

P[failure|x], the conditional probability of failure given the intensity measure $IM = x$, is decomposed in two contributions: the first contribution is due to non-collapse (NC) cases; i.e. to cases where $\delta < \delta_U$, yet larger than the limit-state threshold; the second contribution is due to the collapse (C) cases, i.e. to cases where $\delta > \delta_U$. The conditional probability of failure, given that collapse has occurred and that the intensity measure $IM = x$, *P[failure|x,C],* is equal to one, whichever the limit state and the *IM* are. According to these hypotheses, Equation (5.1) can be re-written as follows (Shome and Cornell, 2000):

$$P[\,failure \mid x] = \Phi^{Comp}_{\delta|IM=x,NC}\left(\frac{\ln\left(\delta_{LS}/\hat{\delta}\right)}{\sigma_{\ln(\delta)}}\right) \cdot P\big[NC \mid x\big] + \big(1 - P\big[NC \mid x\big]\big) \tag{5.2}$$

where $\Phi^{Comp}_{\delta|IM=x,NC}$, providing the probability of conventional collapse, is the standard complementary cumulative normal distribution, $\hat{\delta}$ is the median of data, $\sigma_{\ln(\delta)}$ is the standard deviation of the logarithms, and δ_{LS} is the drift limit to conventional collapse. *P[C|x]=(1 - P[NC|x])* and *P[NC|x]* are computed as the number of collapse and non-collapse cases, respectively, over the total number of records (i.e., thirty) at each IM level. However, it should be noted that the lognormal model (defined for any δ value) may be not perfectly appropriate as, factually, it should not apply for values $\delta > \delta_U$ (recall that these data were not used to determine the parameters of the lognormal distribution). In fact, a truncated model (if data support such a choice) should be used, meaning that the lognormal term at the right hand side of Equation (5.2) should be divided by one minus the exceedance probability of δ_U it provides. Fragility curves for all the considered structural models were computed according to the procedure outlined in the equation, as it was checked that the truncation does not lead to significantly different results. Alternatively, maximum likelihood estimates of the distribution parameters, according to a censored data sample, may also be used.

5.1.1 Three-dimensional model

Results for the three-dimensional model of the 1991 structure ("1991-3D" model, Fig. 1) are shown in Figure 6, where it can be noted that the probability of exceeding the LS limit state is very close to the one for the CP limit state. This is a consequence of the significant influence of P-Delta effects on the 3D model response, as discussed in the companion paper. On the contrary, P-Delta effects have a negligible influence on the IO limit state.

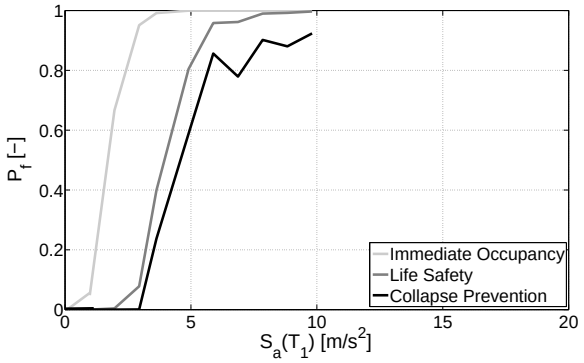

Figure 6. Global fragility curves for "1991-3D" three-dimensional model.

As previously noted (Section 3.2), ground motion records were scaled up to spectral accelerations equal to 1g in case of a 3D model analysis. This explains why the CP limit state fragility curve shown in Figure 6 stops at a value of $P_f < 1$. It is noted that the probability of failure is predominantly affected by the fragility at small-to-medium earthquake intensity, where the hazard assumes significantly larger values (Fig. 2). Therefore, the CP fragility curve was considered sufficiently approximated.

The three-dimensional model is based on the assumption of indefinitely linear elastic response of any roof member, but transverse bracing members hardly can satisfy this model assumption, because of the high slenderness leading to early buckling. Once buckling of transverse roof bracing is triggered, the structure behaviour significantly changes, because frames tend to behave independently each other. This was the reason why to examine the response of a 2D frame model, whose fragility curves are presented in the following section.

5.1.2 Bi-dimensional models

Fragility curves obtained from analysis of 2D frame models are shown in Figure 7*a* and 7*b*, for the 1991 and 1971/79 structures, respectively. Comparing the structural response in the two principal plan directions (*x*- and *y*-directions in Figure 1), it can be noted that, for both the 1991 (Fig. 7*a*) and the 1971/79 building (Fig. 7*b*), fragility curves corresponding to the IO limit state are similar for the two directions, while fragilities at the CP limit state are significantly different. This behaviour is explained based on the period of vibration and the influence of P-Delta effects. The period of elastic vibration is similar in the two directions. At high performance levels, that is, at small earthquake intensities, the demand is sufficiently small to make P-Delta effects negligible. Since the periods of vibration are similar in the two directions and equal to about 1 s for the 1991 and 1.6 s for the 1971/79 building, the displacement demand can be approximately estimated by the "equal-displacement" rule. Thus, the similar values of the fragilities at the IO limit state for the two directions of each building can be justified. When low performance levels are investigated, such as the CP limit state, the significance of P-Delta effects is much more important and can make the difference. Indeed, the sensitivity to P-Delta effects is larger when the earthquake acts along the *x*-direction than it is in case of earthquakes acting in the *y*-direction (Petruzzelli *et al.*, 2012). Consequently, the fragility at the CP limit state is larger for the *x*-direction structure than it is for the *y*-direction structure.

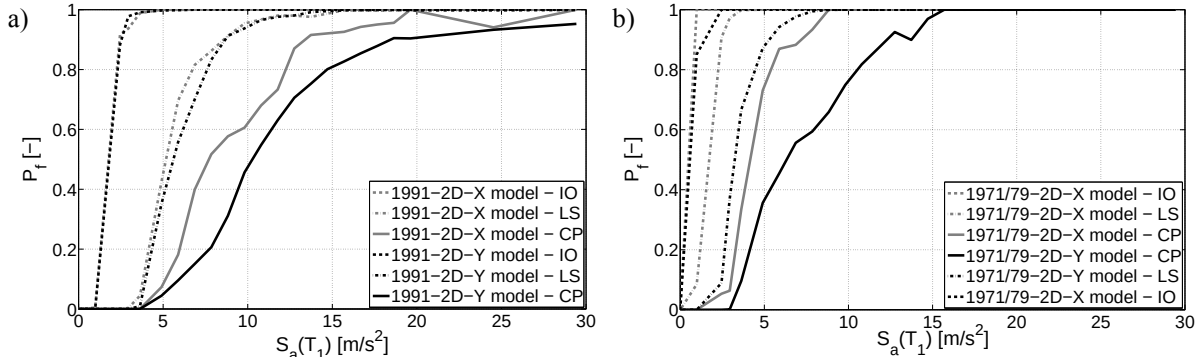

Figure 7. Global fragility curves for 1991 building (a) and "1971/1979" building (b).

Moreover, it is possible to observe that the *x*-direction is, both for the portion built in 1991 and the one built in 1971/79, the most vulnerable direction: the fragility for the *x*-direction is always higher than the fragility for the *y*-direction.

Comparing Figures 7*a* and 7*b*, one could argue that the 1971/79 building is more vulnerable than the 1991 building, whichever is the considered limit state (Petruzzelli *et al.*, 2012). Nevertheless, since the two models present different spectral accelerations at the fundamental period, a comparison of the seismic performance is more appropriate to be done in terms of probabilities of failure.

5.2 Local failure modes (axial force and bending moment)

Failure of members and connections due to excessive force demand has been characterized by a probability of failure obtained, in the frequentistic approach, as the ratio of the number of ground acceleration records inducing a demand larger than the capacity and the total number of records.
This assumption is due to the difficulties in fitting an appropriate probability distribution for force demands, given the IM, due to the particular trend (discussed in Section 4.2) and small dispersion of the demands. Events of global "collapse" in terms of drift were obviously excluded from this calculation. Figure 8 shows examples of fragility curves obtained for two members extracted from the "1991-2D-Y" and "1991-2D-X" model, respectively. Similar curves were obtained for each element of the analysed structural models.
Figure 8*a* corresponds to the case in which the capacity falls between the axial force acting on the member due to gravitational loads and the one corresponding to the lower level of IM. In other words, this is the case of a frame which can withstand gravitational loads, but for a whatever small value of spectral acceleration the probability that the demand exceed the capacity is close to 1. Considering that IMs ranging between 0 and 0.1 g were not investigated (i.e. 0.1 g is the lowest IM value considered), a linear approximation of the fragility curve was adopted in the aforementioned range. The one discussed above, is the case of the weakest elements of all the considered structural models which, therefore exhibit the same fragility curve as the one depicted in Figure 8*a*. Conversely, the case shown in Figure 8*b* is obtained for a capacity falling between the axial force demands at the lower level of IM and those corresponding to the formation of a fully plastic mechanism. Other possible limit cases are: (i) a capacity larger than the axial force obtained at the formation of the plastic mechanism, which corresponds to a probability of failure equal to zero; (ii) a capacity lower than the axial force due to gravitational loads, which corresponds to a probability of failure equal to 1. This latter case never occurs in the analysed models. This behaviour is observed for all the examined structures. Similar considerations apply for the fragility of column base welds.

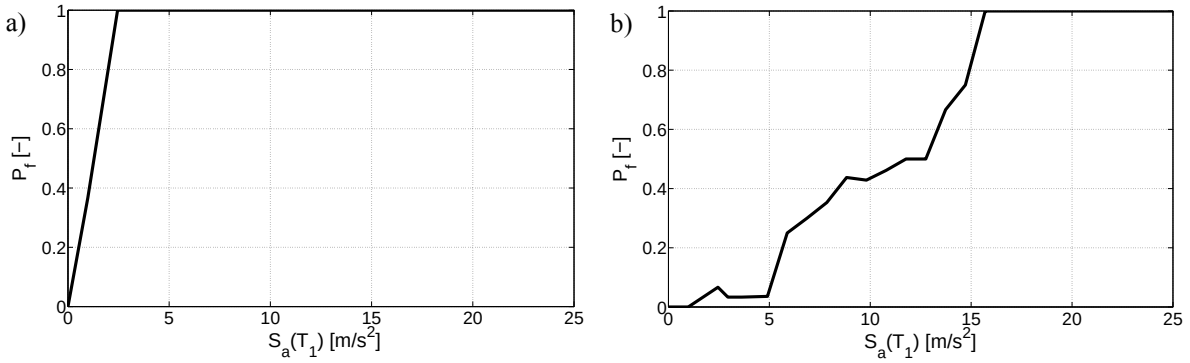

Figure 8. local fragility curves for two members belonging to "1991-2D-Y" (a) and "1991-2D-X" (b) model

6. PROBABILITY OF FAILURE

6.1 Probability of global failure

Once the seismic hazard has been characterized by means of hazard curves at the site (Section 3) and the fragility curves have also been obtained by means of IDA results (Section 4 and Section 5), the probability of failure can be calculated for each of the considered performance levels. The probability of failure, given a limit state ($P_{f,Limit\ State}$), is calculated as reported in Equation (2.1) for all the considered structural models. In the specific case, the hazard curve was calculated in terms of annual probability, therefore, the $P_{f,Limit\ State}$ is the probability that a limit state is reached in period of time equal to one year. Results from the calculations are reported in Table 2. It is worth noting that probabilities of failure may be affected by the approximation of fragility curves in the range of low seismic intensities. In fact, IDAs were performed considering an IM step equal to 0.1 g.

Table 2. Annual probabilities of exceeding global drift ratio limits.

Structure	direction	$P_{f,IO}$	$P_{f,LS}$	$P_{f,CP}$
1991-3D	*y*	5.4E-03	8.5E-04	5.6E-04
1991-2D	*y*	4.8E-03	3.9E-04	1.1E-04
1991-2D	*x*	5.0E-03	4.6E-04	1.8E-04
1971/79-2D	*y*	2.4E-03	3.5E-04	7.2E-05
1971/79-2D	*x*	2.6E-03	1.3E-03	2.0E-04

The probability that the Immediate Occupancy (IO) limit state is reached has the same order of magnitude for the two directions of each examined structure. This can be explained considering that, on one hand, the "1991" building is stiffer than the "1971/79" building and characterised by lower drift demands, as testified by all the structural analysis results, but, on the other hand, the lower flexibility also results into a lower period of vibration (T = 1 s for the "1991" structure and T = 1.6 s for the "1971-1979" structure). Accordingly, the probability of exceeding any given value of the spectral acceleration is higher for the "1991" building. The annual probability of failure, which is the convolution of the two terms (Eqn. 2.1), compensates these two opposite aspects and assumes values of the same order of magnitude. The considerations previously discussed for the IO limit apply in the whole field of stable structural response. When the structure encounters larger displacements, P-Delta effects becomes more important and can change significantly the probability of failure. This phenomenon partially affects the Life Safety (LS) limit state. In fact, the *x*-direction is characterized by larger values of P_f than the *y*-direction both in case of the "1991" and the "1971-1979" structures. This is related to the larger sensitivity of the *x*-directions to the P-Delta effects. The influence of P-Delta effects becomes very large when the Collapse Prevention (CP) limit state is considered. This can be observed comparing $P_{f,CP}$ values with respect those obtained at LS limit state, as well as comparing $P_{f,CP}$ values for the two analysis direction. In fact, the "1971/79" model shows a probability of failure in the *x*-direction one order of magnitude larger than that in the *y*-direction. .

6.2 Probability of local failure

In a similar manner, the probabilities of exceedance of local member capacity were calculated, for each structural member of the bi-dimensional models. Results are shown in Table 3 for the weakest element among roof members and for base plate welds, together with the number of failing elements over the total.

Table 3. Annual probabilities of exceeding local capacity limits.

Structural model	failing elements/ total	P_f of the weakest roof member	P_f of the column base plate welds
1991-2D-Y	10/102	1.06E-02	-
1991-2D-X	36/73	5.1E-02	-
1971/79-2D-Y	5/102	-	1.7E-02
1971/79-2D-X	342/452	1.7E-02	-

It follows that a significant number of elements require strengthening, since the occurrence of local capacity is more probable than the occurrence of global drift performance limits. Even if in modern codes the suppression of such mechanisms is mandatory, the assessment of their probability of failure gives a numerical quantification of the risk deriving from possible local failures. In fact, Table 3 shows that the probabilities of failure associated to local mechanisms are one order of magnitude larger than those related to the immediate occupancy limit state.

7. CONCLUSIONS

Quantitative seismic risk assessment of a case study steel industrial building was addressed in this paper. PBEE approach was followed, considering the uncertainty in ground motion. This latter was addressed performing record selection on the basis of a disaggregation of seismic hazard at the building site. The seismic behaviour of several structural models, extracted from the case study building, was analysed by means of incremental dynamic analyses.
Results were presented in terms of probabilities of exceedance of both global and local failures modes (structural fragility). It was emphasised that fragility curves need to be accurately represented in the field of low seismic intensities, because smaller values of spectral accelerations are much more probable than larger values and they strongly affect the final result in terms of failure probability. The need of suppressing undesired failure modes, such as roof collapse or weld connection failure, emerged as a priority for the case-study building. In fact, probabilities of failure due to such mechanisms resulted to be two order of magnitude larger than that of a global column-sway mechanism.
As a general outcome of the study, it is noted that the probabilistic methodologies appear to be rather well established and consolidated, while guidelines need to be developed for modelling existing structures on a rational basis, especially degradation phenomena.

ACKNOWLEDGMENT
This work was partially supported by AXA-Matrix, within the AXA-DIST 2010-2013 research program, and partially by ReLUIS, within the ReLUIS-DPC 2010-2013 research program.

REFERENCES

ASCE (2000). Pre-standard and Commentary for the Seismic Rehabilitation of Buildings. *Report No. FEMA 356*. Reston, VA: American Society of Civil Engineers prepared for the Federal Emergency Management Agency.

Cornell, C.A., Krawinkler, H., (2000). Progress and challenges in seismic performance assessment. *PEER Center News*, Spring, 2000. http://peer.berkeley.edu/news/2000spring/index.html.

CS.LL.PP. (2008). D.M. 14.01.2008: Norme Tecniche per le Costruzioni. *GU della Repubblica Italiana* **29**,4 febbraio 2008 (in Italian).

FEMA (2000). Recommended seismic design criteria for new steel moment-frame buildings *Report No. FEMA-350*, SAC Joint Ventura, Federal Emercency Management Agency, Washington DC.

Goulet, C.A., Haselton, C.B., Mitrani-Reiser, J., Beck, J.L., Deierlein, G.G., Porter, K.A. and Stewart, J.P. (2007). Evaluation of the seismic performance of a code-conforming reinforced-concrete frame building-from seismic hazard to collapse safety and economic losses. *Earthquake Engineering and Structural Dynamics* **36**, 1973-1997.

Iervolino, I., Galasso, C., Cosenza, E., (2010). REXEL: computer aided record selection for code-based seismic structural analysis. *Bulletin of Earthquake Engineering* **8**, 339-362.

Iervolino, I., Chioccarelli, E., Convertito, V., (2011). Engineering design earthquakes from multimodal hazard disaggregation, *Soil Dynamics and Earthquake Engineering* **31:9**, 1212–1231.

Petruzzelli, F., Della Corte, G., Iervolino, I., (2012). Seismic risk assessment of an industrial steel building, Part 1: modelling and analysis. *15th World Conference on Earthquake Engineering*, Lisbon, Portugal.

Porter, K.A., Kiremidjian, A.S. and LeGrue, J.S. (2001). Asssembly-based vulnerability of buildings and its use in performance evaluation. *Earthquake Spectra* **17:2**, 291-312.

Shome, N., Cornell, C.A., Bazzurro, P., Carballo, J.E., (1998) Earthquakes, records and nonlinear responses. *Earthquake Spectra* **14:3**,469-500.

Shome, N., Cornell, C.A., (2000) Structural Seismic Demand Analysis: Consideration of "Collapse", *8th ACSE Specialty Conference on Probabilistic Mechanics and Structural Reliability*, PMC2000-119.

Vamvatsikos, D., Cornell, C.A. (2002). Incremental dynamic analysis. *Earthquake Engineering and Structural Dynamics* **31**, 491–514.